China Geology 4 (2020) 545−557

China Geology

Journal homepage: http://chinageology.cgs.cn
https://www.sciencedirect.com/journal/china-geology

Occurrence and influence of residual gas released by crush methods on pore structure in Longmaxi shale in Yangtze Plate, Southern China

Ming-liang Liang[a, b, c], Zong-xiu Wang[a, b,*], Guo-dong Zheng[d], Hugh Christopher Greenwell[c], Hui-jun Li[a, b], Lin-yan Zhang[a, b], Xing-qiang Feng[a, b], Kai-xun Zhang[a, b]

[a] *Institute of Geomechanics, Chinese Academy of Geological Sciences, Beijing* 100081, *China*
[b] *Key Lab of Shale Oil and Gas Geological Survey, Chinese Academy of Geological Sciences, Beijing* 100081, *China*
[c] *Departments of Earth Sciences, Durham University, Durham DH*1 3*LE, UK*
[d] *Northwest Institute of Eco-Environment and Resources, Chinese Academy of Sciences, Lanzhou* 730000, *China*

ARTICLE INFO

Article history:
Received 5 March 2020
Received in revised form 4 July 2020
Accepted 29 July 2020
Available online 11 December 2020

Keywords:
Shale gas
Pore structure
Residual gas
Particle size
Fractal dimension
Low-pressure nitrogen adsorption
Oil and gas exploration engineering
Longmaxi shale
Southern China

ABSTRACT

The composition of gas released under vacuum by crushing from the gas shale of Longmaxi Formation in Upper Yangtze Plate, Southern China was systematically investigated in this study. The effect of residual gas release on pore structures was checked using low-pressure nitrogen adsorption techniques. The influence of particle size on the determination of pore structure characteristics was considered. Using the Frenkel-Halsey-Hill method from low-pressure nitrogen adsorption data, the fractal dimensions were identified at relative pressures of 0–0.5 and 0.5–1 as D_1 and D_2, respectively, and the evolution of fractal features related to gas release was also discussed. The results showed that a variety component of residual gas was released from all shale samples, containing hydrocarbon gas of CH_4 (29.58%–92.53%), C_2H_6 (0.97%–2.89%), C_3H_8 (0.01%–0.65%), and also some non-hydrocarbon gas such as CO_2 (3.54%–67.09%) and N_2 (1.88%–8.07%). The total yield of residual gas was in a range from 6.1 μL/g to 17.0 μL/g related to rock weight. The geochemical and mineralogical analysis suggested that the residual gas yield was positively correlated with quartz (R^2=0.5480) content. The residual gas released shale sample has a higher surface area of 17.20–25.03 m^2/g and the nitrogen adsorption capacity in a range of 27.32–40.86 ml/g that is relatively higher than the original samples (with 9.22–16.30 m^2/g and 10.84–17.55 ml/g). Clearer hysteresis loop was observed for the original shale sample in nitrogen adsorption-desorption isotherms than residual gas released sample. Pore structure analysis showed that the proportions of micro-, meso- and macropores were changed as micropores decreased while meso- and macropores increased. The fractal dimensions D_1 were in range from 2.5466 to 2.6117 and D_2 from 2.6998 to 2.7119 for the residual gas released shale, which is smaller than the original shale. This factor may indicate that the pore in residual gas released shale was more homogeneous than the original shale. The results indicated that both residual gas and their pore space have few contributions to shale gas production and effective reservoir evaluation. The larger fragments samples of granular rather than powdery smaller than 60 mesh fraction of shale seem to be better for performing effective pore structure analysis to the Longmaxi shale.

1. Introduction

Natural gas storage in shale reservoirs can be mainly categorized as either adsorbed gas, free gas, or dissolved gas (Curtis GB, 2002); shale rocks are normally a tight reservoir characterized by abundant nanopores and assorted microfractures (Clarkson CR et al., 2016; Ross DJK and Bustin RM, 2008; Loucks RG et al., 2009, 2012; Luo L et al., 2019). For the *in-situ* geological conditions, all the adsorbed and free gas are residual gas left in source rocks after most of the generated gas in mature and over-mature shale migrated into the conventional reservoirs (Curtis GB, 2002; Milkov AV et al., 2020). But in the evaluation of the potential of shale gas in the laboratory, the adsorbed gas is usually obtained by desorption method, while the residual gas is usually defined as the gas obtained by crushing method after the desorption process (Zhang TW et al., 2014; You SG et al., 2015; Wan JB

First author: *E-mail address*: liangmingl09@mails.ucas.ac.cn (Ming-liang Liang).
* Corresponding author: *E-mail address*: wangzongxiu@sohu.com (Zong-xiu Wang).

doi:10.31035/cg2020070
2096-5192/© 2020 China Geology Editorial Office.

et al., 2015). Since residual gas is difficult to extract from the reservoir condition and is of little significance to shale gas production (You SG et al., 2015), the characterization of the residual gas in shale is still insufficient. Nevertheless, the crushing process of obtaining residual gas releases a significant amount of pores (Zhang TW et al., 2014). And, crushing is a common method of sample preparing for the quantitative evaluation of the pore structure of shale, accompanied by the residual gas release and particle size fining. The influence of particle size changes on the pore structure characteristics was determined by lots of researchers (Mastalerz M et al., 2017; Luo L et al., 2019), while the relationship between residual gas and pore structure is still in question.

Pores in shale reservoir are generally divided into micropores (<2 nm), mesopores (2–50 nm), and macropores (>50 nm), according to pore diameter by the classification of International Union of Pure and Applied Chemistry (IUPAC) (Sing KSW et al., 1985; Thommes M et al., 2015). Differences in geological conditions during formation and maturation and material compositions lead to the complexity of pore structures in shale (Clarkson CR et al., 2016; Ross DJK and Bustin RM, 2007, 2008; Chalmers GRL and Bustin RM, 2007; Chalmers GRL et al., 2012; Loucks RG et al., 2009, 2012; Chen F et al., 2018). Properties of nanopore structures in shale are affected by various factors including geochemical conditions and thermal maturity (Curtis ME et al., 2012; Zhang TW et al., 2012; Sun LN et al., 2015), lithology and diagenesis (Ross DJK and Bustin RM, 2009; Chalmers GRL and Bustin RM, 2008; Chalmers GRL et al., 2012), tectonic process and texture deformation (Liang ML et al., 2017; He JL et al., 2018; Ju YW et al., 2018), and sample preparing and particle fining (Mastalerz M et al., 2017; Luo L et al., 2019).

Termed as “organic-rich” rock, organic matter (OM) and its geochemical evolution in shale were generally considered as the primary factor controlling pore structures of shale (Clarkson CR et al., 2016; Curtis ME et al., 2012; Zhang TW et al., 2012; Sun LN et al., 2015; Ross DJK and Bustin RM, 2009; Chalmers GRL and Bustin RM, 2008; Chalmers GRL et al., 2012). Chalmers GRL et al. (Chalmers GRL and Bustin RM, 2007, 2008; Chalmers GRL et al., 2012) studied the pore characteristics of shale from North American with different total organic carbon (TOC) and mineral compositions and found that the samples contained higher quartz, moderate clay, and high TOC content displayed more equally weighted ratios between micro-, meso- and macroporosity. These studies indicated that the TOC content alone was not enough to predict pore structure (Chalmers GRL and Bustin RM, 2008; Chalmers GRL et al., 2012). Compared to the US shale basins, the correlation between the TOC content and nanopore structure was stronger and more predictable in Lower Paleozoic shale from Southern China (Zhai GY et al., 2018a, 2018b). This difference may be caused by the different thermal maturity of shale between Northern American (R_o=0.4%–1.9%) and Southern China (R_o>2.0%) (Nie HK et al., 2009), and indicated that TOC content alone was not enough to predict porosity in nanopores, but other factors like OM composition, kerogen, and thermal maturity also need to be considered (Curtis ME et al., 2012; Zhang TW et al., 2012; Sun LN et al., 2015). Solid organic matter (SOM) acts as a harmful factor to pore structure development in shale, with nanoscale porosity increasing after SOM removal and the micropore has a remarkably higher than meso- and macropores (2–200 nm) (Li J et al., 2016). With the evolution of each thermally mature stage, from immaturity to high maturity, kerogen is lost while porosity increases (Sun LN et al., 2015), and the formation and evolution of nanopores occurs upon the generation and expulsion of hydrocarbon fluids (oil and gas) during the thermal maturation processes (Curtis ME et al., 2012; Zhang TW et al., 2012; Sun LN et al., 2015). Extractable organic matter (EOM, residual oil and bitumen) can also occupy the pores in shale and influence the pore structure (Li J et al., 2016). The number of nanopores increased significantly after the removal of EOM during organic solvent extraction of shale. Although the effect of OM (solid OM, kerogen, residual oil, and bitumen) and its evolution on pore structure in shale have been described in previous studies (Curtis ME et al., 2012; Zhang TW et al., 2012; Sun LN et al., 2015; Li J et al., 2016), the amount and location of hydrocarbon gas in shale, and its influence on pore structure, remains poorly understood. A challenge to studying gas in shales arises due to the dynamic nature of the gaseous fluid in shale reservoirs under geological conditions. The interaction between gas storage location, mode of binding, and pore structure properties are coupled. Hydrocarbon gas undergo desorption and release from shale when the pore structure of the reservoir is changed during hydraulic fracturing. While hydrocarbon gas adsorption will induce shale swelling (Chen TY et al., 2015), it may cause pore structure change within the shale. Recently, research on residual gas within shale was studied by a vacuum rock crushing method to investigate gas potential and gas storage mechanisms in shale. The residual gas geochemical characteristics indicated that the gas storage in Niutitang shale was mostly generated from the cracking of residual bitumen and wet gas during the high maturity phase of development (Wu CJ et al., 2016; Yang YR et al., 2019). Both thermal maturity and gas desorption contributes to change in the gas composition of gas released during rock crushing from nine samples of Barnett shale (Zhang TW et al., 2014), revealing that gas occupancy is an important factor in determining pore structure that can not be ignored. However, a comprehensive understanding of the effect of gas on pore structure remains to be elucidated, and residual gas analysis technology provides an opportunity to address this question. Therefore, determining the influence of residual gas release on pore structure properties is of great importance to understand the gas storage and nanopore structure in organic-rich shale, and would be beneficial towards providing a new strategy for pore structure studies.

In this study, organic-rich shale samples from the

Longmaxi Formation in the Upper Yangtze, Southern China were studied. The geochemical composition of residual gas was measured, and nanopore structural feature investigations were performed using low-pressure nitrogen (N_2) adsorption. The effect of residual gas on the pore structure was studied by N_2 adsorption data and fractal dimensions. The relationship between shale composition and residual gas yield is discussed. The influence of particle size on pore structure has also been considered, owing to the residual gas released samples being collected by crushing methods, with more fine-grinding associated particle size. These experimental results provide valuable information and implications for pore parameters of residual gas in a shale reservoir, which is beneficial to provide a new strategy for pore structure studies on gas shale.

2. Samples and methods

2.1. Samples setting

The Longmaxi Formation is the leading target for shale gas exploration and development in China, which is widely distributed in the Yangtze Plate. Commercially viable shale gas was produced within the Longmaxi shale, from the Fuling area and Changning-Weiyuan area in the Upper Yangtze platform, Southern China (Zhai GY et al., 2018a, 2018b; Zhou Z et al., 2018; Yang YR et al., 2019; Meng FY et al., 2020). Shale samples in this study were collected from outcrops of the Longmaxi Formation. The sampling site in Yongshun County is located in the Northwest of Hunan Province, which belongs to the edge of the Upper Yangtze platform (Chen TY et al., 2015; Tan JQ et al., 2014). The sampling location and outcrop photograph are shown in Fig. 1. More detailed information on the stratigraphy, geological, and tectonic condition of samples obtained can be found in the literature (Liang ML et al., 2017).

Before analysis, each sample was cut into fragments of 5–10 mm and then divided into three parts. The first part was crushed to pass through 180–200 mesh for geochemical and mineralogical shale composition analyses. The second part was crushed to 30–50 mesh. Previous studies showed when particle size is greater than 60 mesh, the proportions of gas and CH_4 released from the shale were small, less than 10% (Zhang TW et al., 2014). Thus this second part of the original sample can be named the original (O) shale sample and was submitted for pore structure analysis by N_2 adsorption. The

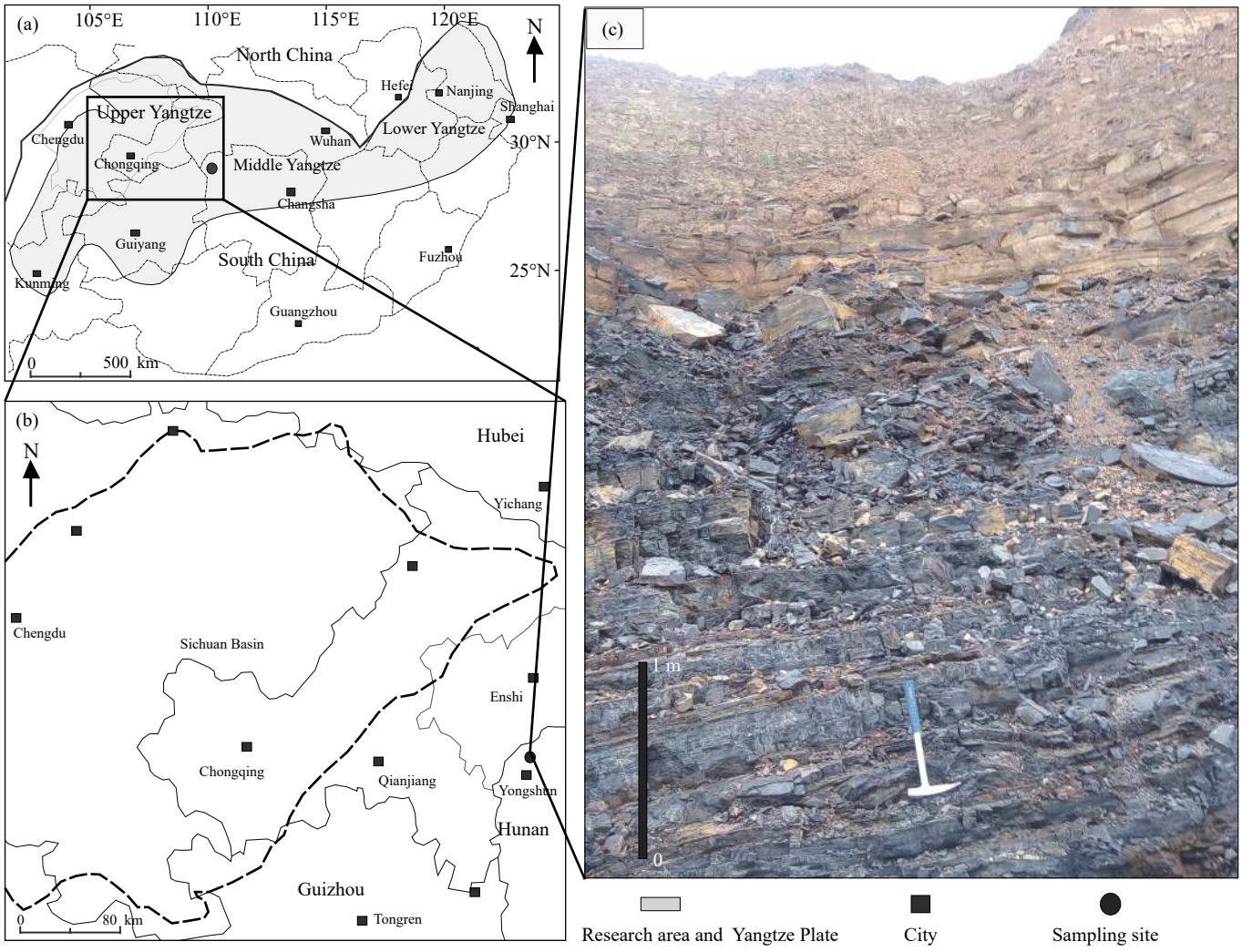

Fig. 1. Map showing the location and outcrop photograph of the study area in Yongshun County, Hunan Province, Southern China.

third part was crushed to 100–200 mesh by the vacuum crush device and named as the residual gas released (R) shale sample for pore structure analysis. The gas released were collected for gas composition analysis by gas chromatography.

2.2. Experimental methods

2.2.1. TOC and mineralogical analysis

The TOC content was measured with a Leco C/S-344 Carbon/Sulfur analyzer after samples were treated with 10% hydrochloric acid to remove carbonate. The mineral composition was measured using a D/Max-III analyzer for X-ray diffraction (XRD) analysis. The relative contents of mineral compositions were semi-quantified using the area under the curve for the major peaks.

2.2.2. Geochemistry of residual gas

The residual gas from the shale was collected and measured using a combined device (Fig. 2) with a high vacuum rock crusher coupled with gas chromatography (GC) with a pulsed discharge detector (PDD). The vacuum of the equipment pipeline can achieve lower than 10^{-4} Pa (Li LW et al., 2017). The combined gas chromatography with a pulsed discharge detector (GC-PDD) gave a high sensitivity gas chromatography analysis of the chemical composition of gas released from rocks (Li LW et al., 2015, 2017). Approximately 3–5 g gravel size rock sample was loaded into the crushing device, evacuated until the pressure was steady at less than 10 Pa. Samples were crushed for 3–5 minutes until the majority of residual gas were released, with the pressure kept steady at about 100–300 Pa, which is related to the released gas yield. The pipeline was evacuated and the gas was released from the crusher into the GC-PDD for gas composition analysis. The sample powder was collected and sized, and the particle size was generally in the range at 100–200 mesh, indicating that the majority of the residual gas were released by crushing (Zhang TW et al., 2014), and those post-crushed samples set as the residual gas released shale samples.

2.2.3. Low-pressure N_2 adsorption analysis

The original shale samples and residual gas released shale samples weighing about 0.3 g were dried at 110°C in a vacuum for 20 h to remove moisture. Subsequently, the low-pressure N_2 absorption measurement was conducted at –196°C using a Micromeritics ASAP 2020 HD88 analyzer. N_2 absorption data were interpreted using Brunauer-Emmett-Teller (BET) analysis for surface area, and density function theory (DFT) for pore volume and pore size distribution. N_2 absorption analysis is primarily used to study the nanopore structure within shale samples (Clarkson CR et al., 2016; Thommes M et al., 2015; Sun LN et al., 2015; Li J et al., 2016). These analyses and calculations have been described previously (Barrett EP et al., 1951; Horvath G et al., 1983; Rouquerol F et al., 1999), and were generated automatically by the software.

2.3. Fractal theory

The fractal dimension calculated using low-pressure N_2 adsorption data had been proved to be a useful parameter to depict the heterogeneity of the pore structure of irregular porous solids (Mahamud MM et al., 2008). In this study,

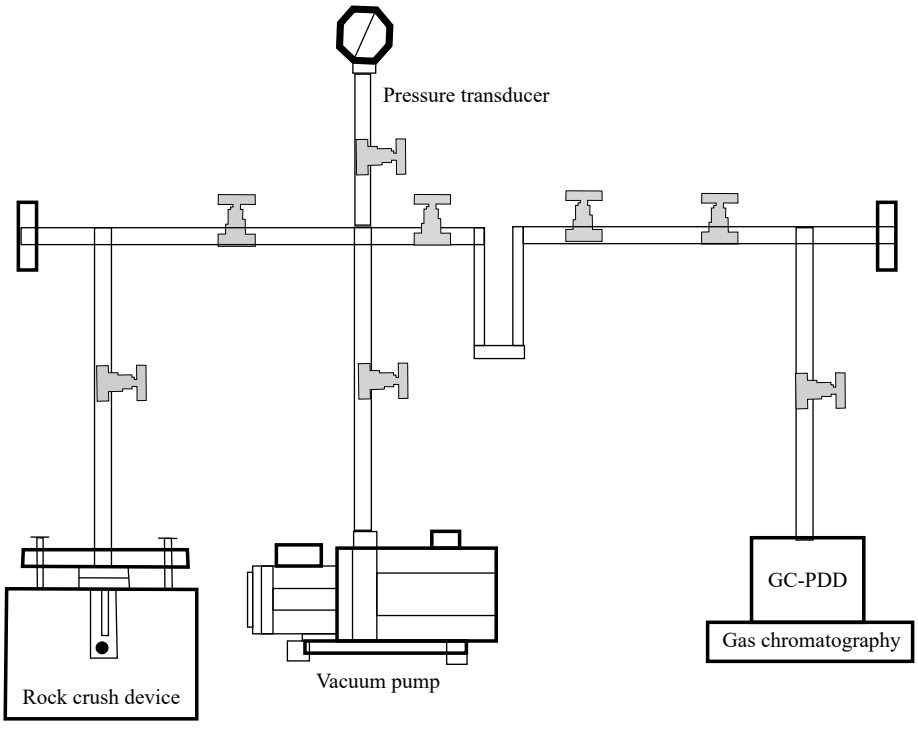

Fig. 2. Schematic diagram of the experimental device for the analysis of released gas with gas chromatography.

fractal dimension was calculated using the Frenkel-Halsey-Hill (FHH) model (Ismail IMK and Pfeifer P, 1994; Qi H et al., 2002; Cao TT et al., 2016; Jaroniec M, 1995), and the equation can be described as follows:

$$\ln(V/V_0) = K\ln[\ln(P_0/P)] + C \quad (1)$$

C is the constant of gas adsorption. The value of K can be obtained by plotting the N_2 adsorption isotherm data in terms of ln (V/V_0) versus ln[ln(P_0/P)]. If the pores in the material were fractal, the fractal dimension (D) value can be obtained from the line slope K:

$$K = D - 3 \quad (2)$$

The value of fractal dimension generally ranges from 2 to 3, where D=2 represents a smooth surface or homogenization of pores and D=3 corresponds to a rough surface or totally heterogeneity of pore structure (Cao TT et al., 2016; Jaroniec M, 1995). Based on the N_2 adsorption isotherm data, two distinct linear segments at relative pressures of 0 –0.5 and 0.5–1 were obtained as D_1 and D_2, respectively.

3. Results and discussion

3.1. TOC and X-ray diffraction analysis

The results of TOC content and X-ray diffraction analysis for all original shale samples are shown in Table 1. The TOC content and mineralogical composition of shale are believed to be important properties controlling pore structure and gas storage in shale (Sun LN et al., 2015; Ross DJK and Bustin RM, 2009; Chalmers GRL et al, 2008, 2012). All samples showed relatively high TOC content, ranging between 2.77% and 3.77%, with an average value of 3.43%, and displayed high-quality organic matter rich features, and confirmed that all samples were collected from the organic-rich formation (TOC >2%) from the base of the Longmaxi Formation. The measured vitrinite reflectance values (R_o %) for the same outcrop samples have been reported previously (Liang ML et al., 2017), and were found to be within the dry-gas generation window (R_o values of 2.6% to 3.0%). These results suggested that the shale samples have high-quality organic matter richness for shale gas generation over geological time, providing the material basis for residual gas. Mineral assemblages in the studied samples are dominated by quartz (55.1%–72.7%, average 64.8%) and clay minerals (14.4%–23.9%, average 18.5%). The quartz was classified as biogenic siliceous, due to the high quartz contents above 55% correlated with high TOC content above 2.7%. Evidence for graptolite and radiolarians provides high levels of biogenic siliceous and organic carbon at the bottom of Longmaxi shale (Luo QY et al., 2016). In addition to the contribution of biogenic silicon, the parts of extra quartz content may come from the hydrothermal source, after the tectonic process and fracture generations as fracture filling in of shale (Liang ML et al., 2017).

Table 1. TOC content and mineralogical composition of the shale samples (%).

Sample	YS1701	YS1702	YS1703	YS1704	YS1705	YS1706
TOC	3.69	3.66	3.65	3.77	2.77	3.06
Quartz	64.2	59.0	72.7	70.4	55.1	67.3
Feldspar	5.7	4.9	4.0	7.9	9.4	8.9
Carbonate	1.4	9.9	5.8	1.4	7.0	1.6
Pyrite	2.5	2.8	1.6	5.8	7.0	4.8
Total caly	23.9	21.3	15.2	14.4	18.9	17.4

3.2. Geochemical characteristics of residual gas

The residual gas yield and its geochemical composition are lists in Table 2. The absolute gas yields (include non-hydrocarbon gas) are in the range of 6.1 –17.0 μL/g rock (average 11.7 μL/g rock), dominated by CH_4 (29.58%–92.53%, average 69.56%) and CO_2 (3.43%–66.43%, average 22.19%), with minor ethane (0.97%–2.89%), propane (0.01%–0.43%) and nitrogen (1.88%–8.07%), detected. This residual gas yield is about less than 1% of the produced gas content (1–5 m^3/t) from general shale gas play in Longmaxi gas shale (Guo TL, 2016; Wang QT et al., 2015). The yields of gas released by the crush method were too low to be used to evaluate the potential gas in place (GIP) in the shale gas play (Wang QT et al., 2015). CH_4 and CO_2-rich gas that co-exist in these shales are similar to the residual gas previously described in studies from the Barnet shale (Zhang TW et al., 2014), Niutitang shale (Wu CJ et al., 2016), and Longmaxi shale (Wang QT et al., 2015). The wetness of residual gas (molar fraction of ethane to pentanes in total gaseous hydrocarbon) was 1.47%–4.65%, indicating the residual gas was the result of the gas accumulation from the hydrocarbon source rock during the high maturity period. Moreover, the wetness value (1.47%–4.65%) is within the dry-gas window (Dai JX et al., 2014), and different from that observed in the produced gas (0.24% –0.70%) from the Longmaxi shale after hydraulic fracturing (Dai JX et al., 2014; Cao CH et al., 2015). This might be due to the that in the produced gas, free gas dominates, while in the residual gas adsorbed and trapped gas dominates (Zhang TW et al., 2014; Wang QT et al., 2015). It may suggest that the residual gas in the Longmaxi shale was difficult to release by hydraulic fracturing. Therefore, the pore spaces occupied by residual gas may be the most stable

Table 2. Chemical composition (normalized to 100%) of gas released from shale samples.

Sample	YS1701	YS1702	YS1703	YS1704	YS1705	YS1706
TOC/%	3.69	3.66	3.65	3.77	2.77	3.06
CH_4/%	92.53	91.73	86.39	29.58	72.80	54.58
C_2H_6/%	0.97	1.62	1.20	1.07	2.89	2.02
C_3H_8/%	0.43	0.65	0.09	0.38	0.01	0.15
CO_2/%	3.54	3.68	8.09	67.09	17.85	35.18
N_2/%	2.53	2.32	4.22	1.88	6.45	8.07
Wetness/%	1.49	2.41	1.47	4.67	3.83	3.82
C_1/CO_2	26.13	24.90	10.68	0.44	4.08	1.55
Total released gas/(μL/g rock)	12.0	9.9	13.6	11.4	6.1	17.0

storage space and contains important geochemical information in the stage of shale gas generation and accumulation for the Longmaxi shale.

TOC content is one of the commonly used indicators for the gas potential for shale (Clarkson CR et al., 2016; Ross DJK and Bustin RM, 2007; Chalmers GRL and Bustin RM, 2007; Wu CJ et al., 2016). OM-pore and micropore, interrelated with TOC, are often regarded as the main space where adsorbed gas and/or residual gas exists (Chalmers and Bustin, 2007; Wu CJ et al., 2016). Here, sample YS1705, with the lowest observed TOC of 2.77 %, contains the least gas yield of 6.1 μL/g rock and may be interpreted as supporting the above view. The correlation analysis showed that there was no clear relationship between TOC content and residual gas yield for all samples (R^2 = 0.049). It suggested that the residual gas may also release from other pores besides OM-pores. Fig. 3 shows the correlation between residual gas yield and shale compositions for different minerals and TOC, indicating the positive relationship between gas yield and quartz content (R^2=0.548) and a slightly positive relationship with carbonate.

Under the influence of multi-phase basin evolution and tectonic rebuilding processes, the Longmaxi shale developed multi-layer structural deformation (Liang ML et al., 2017; Guo TL, 2016). The deformation and fractures are thus commonly present in Longmaxi shale samples (Liang ML et al., 2017; He JL et al., 2018), with most fractures filled with quartz and/or calcite (Liang ML et al., 2017; He JL et al., 2018; Gao J et al., 2015). The previous studies (Gao J et al., 2015, 2017) have revealed that fluid inclusions occur as Fluid Inclusion Assemblages (FIA), representing several fluids that were trapped within the mineral fractions (quartz primarily) of the Longmaxi shale. Using Raman spectroscopy analysis, researchers (Gao J et al., 2015, 2017) found that the inclusion contained high-density hydrocarbon gas and non-hydrocarbon fluid, and CO_2 is also found in inclusions. These results suggested that the gas come from the closed pores of the inclusions, which have similar gas composition to the residual gas obtained by the crushing shale and may contribute to the residual gas found in the Longmaxi shale in this present study. This fraction of the gas existed in closed pores in brittle quartz and is difficult to produce by hydraulic fracturing. This stable residual gas less than 1% of the produced gas yield (1–5 m^3/t) and may be meaningless for commercial production in the Longmaxi shale. However, it is precisely because it is not easy to destroy that more geochemical and tectonic information about shale gas reservoirs may be retained in the residual gas, and needs to be studied further in the future.

3.3. Effect of residual gas released on pore structure

3.3.1. N_2 adsorption and desorption isotherms

Low-pressure nitrogen isotherms for original (O) and residual (R) gas released shale samples are shown in Fig. 4. The nitrogen adsorption-desorption curve of shale can be used to analyze the nano-pore structure characteristics (Clarkson CR et al., 2016; Thommes M et al., 2015; Sun LN et al., 2015; Li J et al., 2016). Because capillary condensation and capillary evaporation often do not occur at the same pressure, there is a detached portion between the corresponding desorption and adsorption isotherm branch. According to the classification of the IUPAC (Thommes M et al., 2015), the hysteresis loop pores are divided into four types. The hysteresis loop was observed for all samples, with the desorption branch always above the adsorption branch. However, there was a clear difference between the original (O) and residual (R) gas released shale samples. The shapes of the hysteresis loop in original samples are clear, and similar to the H2 type, suggesting narrow throats between large pore spaces (also named ink-bottle shaped pores). The narrow hysteresis loop shape of samples with residual gas released can be identified as type H3 (or both characteristics of type H2 and H3), indicating silt- and plate-like pores. When the relative pressure P/P_0 was close to 1, the nitrogen adsorption quantities of gas released samples were about 27.32 mL/g to 40.86 mL/g, which were significantly higher than that of the original samples, which were about 10.84 mL/g to 17.55 mL/g. Such dramatic changes of adsorption capacity were observed by Li J et al. (2016), with the extractable organic matter and/or solid organic matter extracted, the nitrogen quantity adsorbed increased significantly for all samples, even with different TOC content. It has been shown that the sample with smaller particle size always has higher adsorption capacity than those samples with bigger size, from the same original shale (Mastalerz M et al., 2017; Luo L et al., 2019; Gao L et al., 2018). Several studies have suggested that the crushing and analytical particle size not only alters the shape of the gas adsorption-desorption hysteresis loop but also affected the pore structure and adsorption capacity of shale (Mastalerz M et al., 2017; Luo L et al., 2019). However, the factors controlling gas release during crushing and fine-grinding of particles have thus far not been considered. These experimental results show that the release of residual gas should also be considered as an influencing factor, which contributes to the improvement of shale adsorption capacity and the change of hysteresis loop, by releasing a certain amount of adsorption surface area and pores.

3.3.2. Pore volume, surface area, and pore size distribution

Characteristic data of pore size distribution, surface area, and pore volume obtained from original and residual gas released shale samples are listed in Table 3 and Table 4. On the whole, the BET surface areas and DFT pore volumes increase after gas release. The BET specific surface of residual gas released shale samples range from 17.20 m^2/g to 25.03 m^2/g with mean values of 21.07 m^2/g, significantly higher than original shale samples range from 9.22 m^2/g to 16.30 m^2/g with an average of 12.46 m^2/g. The development of DFT models has led to a better understanding of adsorption processes in well-ordered systems compared to the more conventional models (Thommes M et al., 2015; Groen JC et al., 2003). The DFT accumulative pore volume of original

shale samples (8.09% –25.63%, average 15.69%) increased after residual gas release (15.59%–26.71%, average 20.93%). Note that the maximum growth rate of surface area, pore volume and N_2 quantity adsorbed (107.29%, 230.16%, and 173.49%, respectively) happen to sample YS1704 after residual gas release, while the highest enrichment of CO_2 in residual gas released was also from sample YS1704, too. This result might not be a coincidence. By studying the chemical and isotopic composition of residual gas released by crush methods from the Barnet shale, Zhang TW et al. (2014) found that the CO_2-rich gas was hosted within the smaller pores than CH_4-rich gas. These studies suggesting that the variation in the composition of residual gas has an important relationship with the pore structure in shale.

The pore volumes related to pore size distribution were derived by analysis of the N_2 adsorption data by DFT.

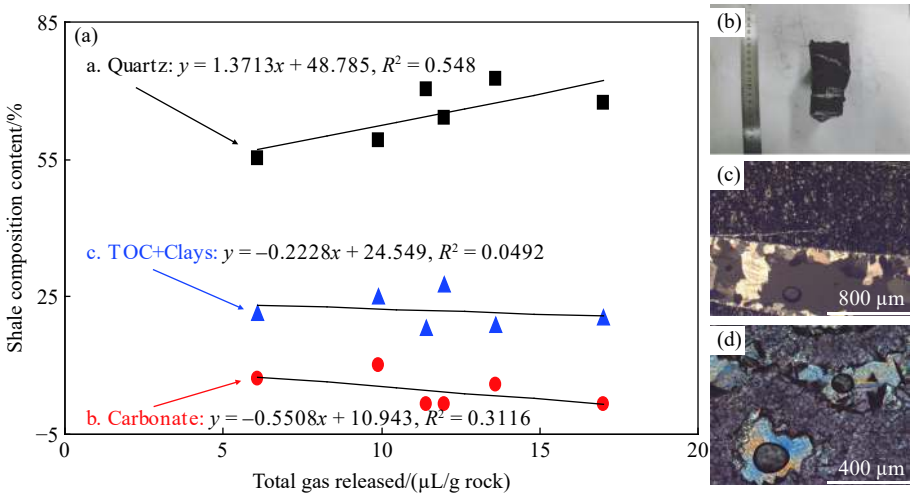

Fig. 3. a–Relationship between shale compositions and residual gas yield of shale samples; b–Longmaxi shale with fracture filling; c, d–inclusions developed in fracture filling of Longmaxi shale.

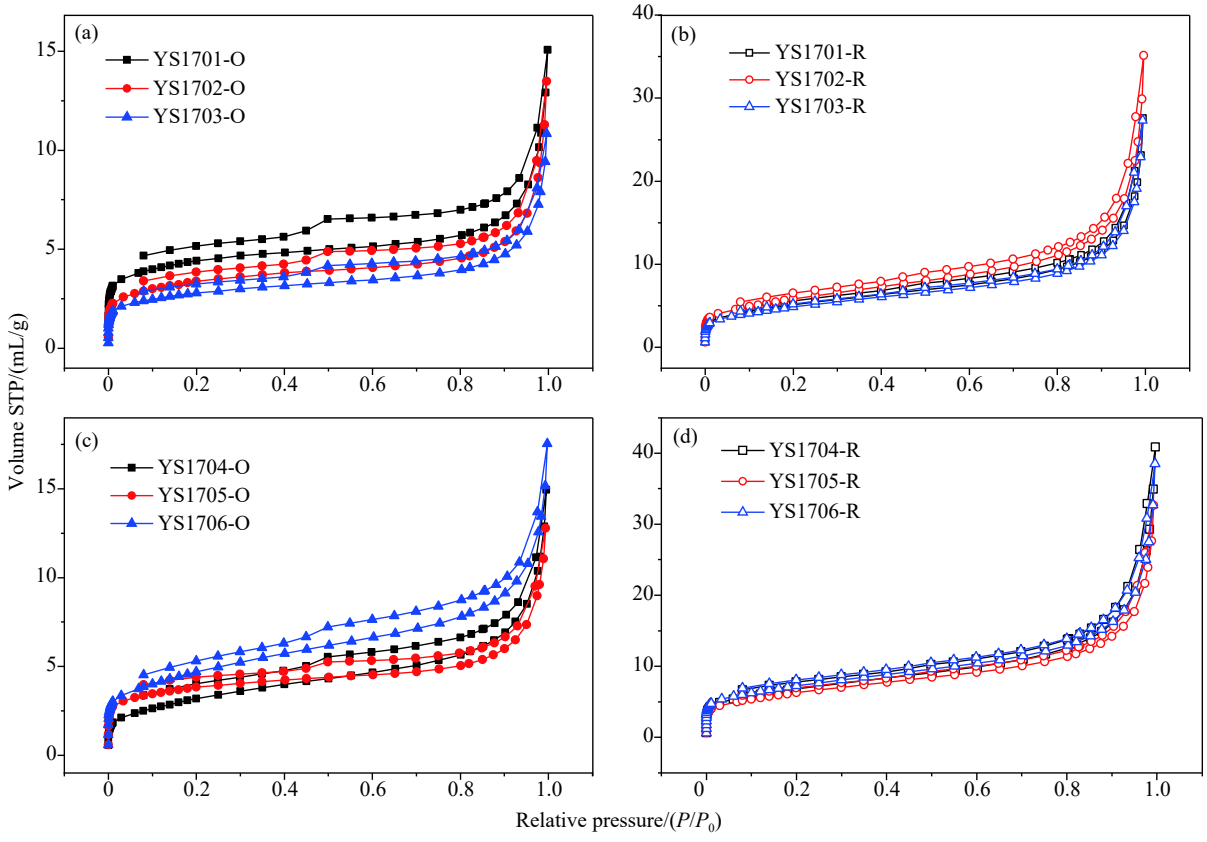

Fig. 4. Isotherms of nitrogen adsorption and desorption for original (O) (a, c) and residual gas released (R) shale samples (b, d). The desorption branch always above the adsorption branch. A significant hysteresis loop and larger detachment were observed for original shale samples than residual gas released shale.

Table 3. Pore characteristic data of original and residual-gas released shale samples.

Sample	Original			Residual-gas released		
	S_{BET}/ (m^2/g)	V_{DFT}/ (μL/g)	Quanity adsorbed/ (mL/g STP)	S_{BET}/ (m^2/g)	V_{DFT}/ (μL/g)	Quantity adsorbed/ (mL/g STP)
YS1701	14.25	21.27	15.06	18.07	15.59	27.57
YS1702	11.17	14.92	13.49	20.59	22.09	35.12
YS1703	9.22	9.95	10.84	17.20	17.59	27.32
YS1704	11.39	8.09	14.94	23.61	26.71	40.86
YS1705	12.40	14.28	12.78	21.89	20.12	32.64
YS1706	16.30	25.63	17.55	25.03	23.48	38.49

According to Fig. 5, the incremental curves from the DFT model versus pore diameter results perfectly reflect pore size distribution for all samples, with and without gas released. A multimodal pattern of pore size distribution is displayed, with major peaks at less than 2 nm, 2.5–3.5 nm, 10–80 nm, and 100–200 nm (Fig. 5), illustrating those pores contribute mainly to the pore volumes of the Longmaxi shale. Meanwhile, pores with pore diameters from 10–80 nm and 100–200 nm were significantly increased and dominate the pore volumes after the residual gas was released by the crush method. According to the classification of IUPAC (Thommes M et al., 2015), pores can be classified into micro-, meso- and macropores using N_2 adsorption data. Pore structure analysis showed that the proportions of micro-, meso- and macropores were changed with micropores decreased, while meso- and macropores increased after the residual gas was released (Fig. 6). The results indicated that the residual gas was mainly released from the mesopores and macropores, and the pore space characterized as micropores in the original samples also changed after particle fine-grinded and the residual gas was released.

3.3.3. Fractal dimensions

A fractal dimension (D) can be applied to characterize pore geometry by quantitatively evaluating parameters such as pore surface roughness and structural irregularity (Mahamud MM et al., 2008; Ismail IMK and Pfeifer P, 1994; Qi H et al., 2002; Cao TT et al., 2016; Jaroniec M, 1995). The value of fractal dimension generally ranges from 2 to 3, where D=2 represents a smooth surface or homogenization of pores and D=3 corresponds to a rough surface or heterogeneity of pore structure (Cao TT et al., 2016; Jaroniec M, 1995). Based on the N_2 adsorption isotherm data, a scatter diagram of ln (V/V_0) versus ln[ln(P_0/P)] can be drawn for the shale samples (Fig. 7). Two distinct linear segments at relative pressures of 0–0.5 and 0.5–1 were obtained as D_1 and D_2, respectively. Based on different adsorption characteristics at different pressure ranges (Yao Y et al., 2008), the fractal dimension D_1 at lower relative pressures of 0–0.5 characterizes the action of Van der Waals forces and reflects the surface fractal dimension. The fractal dimension D_2 at higher relative pressure corresponds to the action of capillary condensation and represents the pore structure fractal dimension. The fractal dimensions D_1 and D_2 were calculated at the relative pressure (P/P_0) range of 0–0.5 and 0.5–1 using the FHH equation. The fitting equations, correlation coefficients of R^2, and fractal dimension values (D_1 and D_2) are summarized in Fig. 7 and Table 5. The D_1 values were always lower than D_2 for each shale sample, consistent with previous research (Yao Y et al., 2008), indicating that the larger pores have a rougher pore surface and more complex pore structure than smaller pores. The fractal dimensions D_1 range from 2.5466 to 2.6117 (average of 2.5732) and D_2 range from 2.6998 to 2.7119 (average of 2.7085) for residual gas released shale, and smaller than the original shale (D_1 range from 2.5171 to 2.7290 with an average of 2.6545, D_2 range from 2.7415 to 2.8046 with an average of 2.7677), indicating that the pores in the residual gas released shale was more homogeneous than the original shale.

3.4. Implication of residual gas and its pore space

It is believed that the particle size affected the pore structure character (Mastalerz M et al., 2017; Luo L et al., 2019), while the residual gas was released with the process of particle fine-grinding by crush methods (Wu CJ et al., 2016; Zhang TW et al., 2014; Li LW et al., 2017; Wang QT et al., 2015). In the previous analysis, the residual gas and nano-pore characteristic obtained by N_2 adsorption data were analyzed. The results show that the pore volume, BET surface area, pore size distribution (ratio of micro-, meso- and macropores), pore geometry (by fractal dimensions) have changed after the residual gas was released by crush methods. These changes are related to the fine-ground sample size obtained by crushing. Meanwhile, the release of gas occurred and released an amount of pore space, which was originally occupied by the residual gas. The residual gas test found that the gas volume is very small as 6.1–17.0 μL/g rock (average 11.7 μL/g rock) and less than 1% (Guo TL, 2016; Wang QT et al., 2015). While the released pore space after gas release and crushing is large (Table 3). Some of the residual gas

Table 4. Pore volume distribution (DFT) of micro-, meso-, and macropores for original and residual-gas released shale samples.

Sample	Original shales			Residual-gas released shales		
	Micropore/(μL/g)	Mesopore/(μL/g)	Macropore/(μL/g)	Micropore/(μL/g)	Mesopore/(μL/g)	Macropore/(μL/g)
YS1701	3.45	8.49	8.39	1.01	6.87	6.62
YS1702	2.11	5.23	6.80	1.06	10.69	9.09
YS1703	1.96	3.53	4.04	0.91	6.77	8.88
YS1704	1.03	4.00	2.73	2.10	12.71	10.87
YS1705	2.71	5.43	5.29	1.48	8.21	9.10
YS1706	2.44	13.18	9.03	2.60	10.61	9.28

occupied pores mainly closed pores as inclusions, which should be considered as ineffective pores for reservoir evaluation. It can be concluded that there are two possible mechanisms which can explain the effect of residual gas released on changes in pore structure by the crush methods: (1) Residual adsorbed gas released from organic matter-related pores (ink bottle-shaped pores), pores destroyed and released, and change of morphology from ink bottle-shaped micropores to slit-shaped mesopores and even macropores; (2) residual inclusion gas released from closed pores (mostly quartz inclusions in the Longmaxi shale), pores released as mesopores and macropores. Considering the influence of factors on the residual gas released also makes it more reasonable to understand the effect of particle size on the pore structure. Fig. 8 deduces the possible influencing mechanisms of residual gas released by the crushing method on the pore

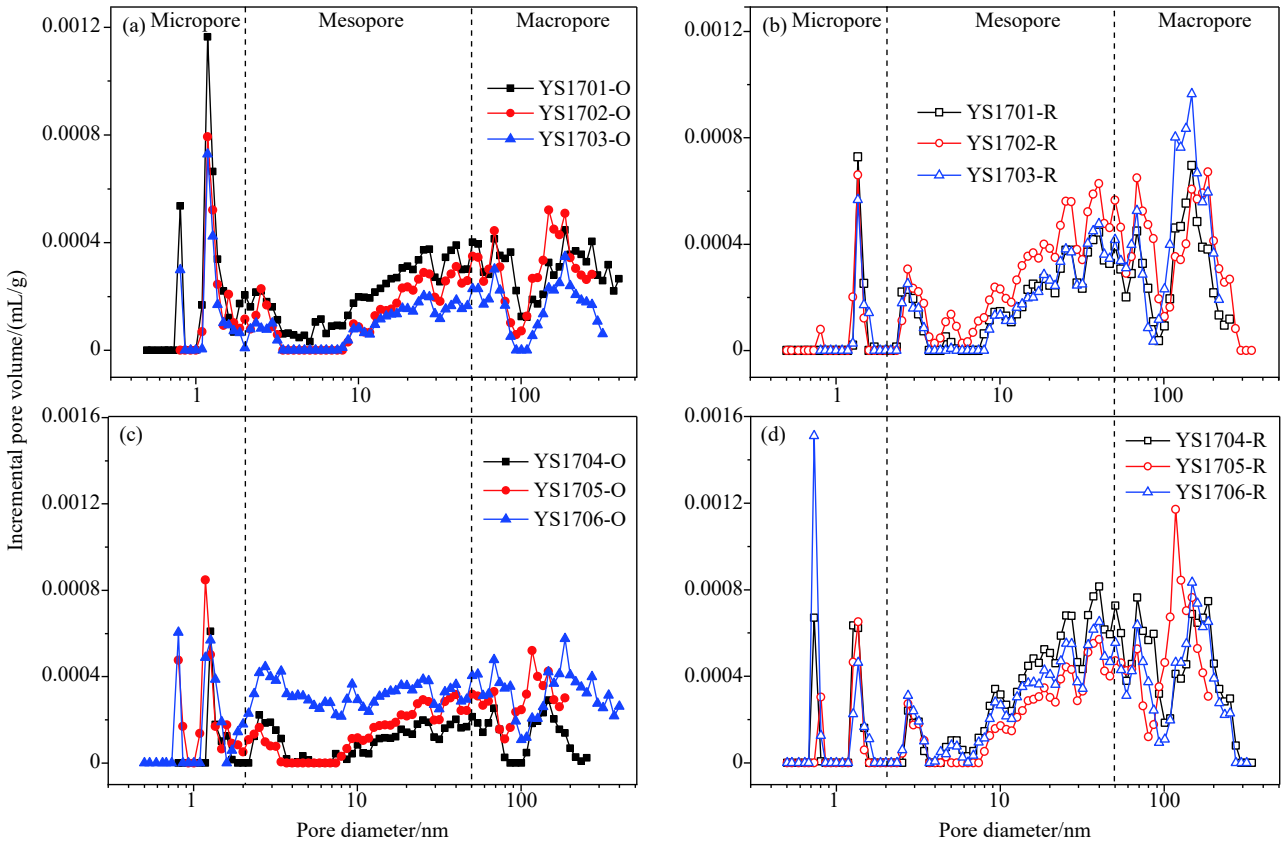

Fig. 5. Pore size distribution is defined by incremental pore volume by DFT methods. Pore diameters range between 0.4 nm and 300 nm. The boundaries between micro-, meso- and macropores are highlighted by dashed lines. a, c–pore size distribution for original shale samples; b, d–pore size distribution for residual gas released shale samples.

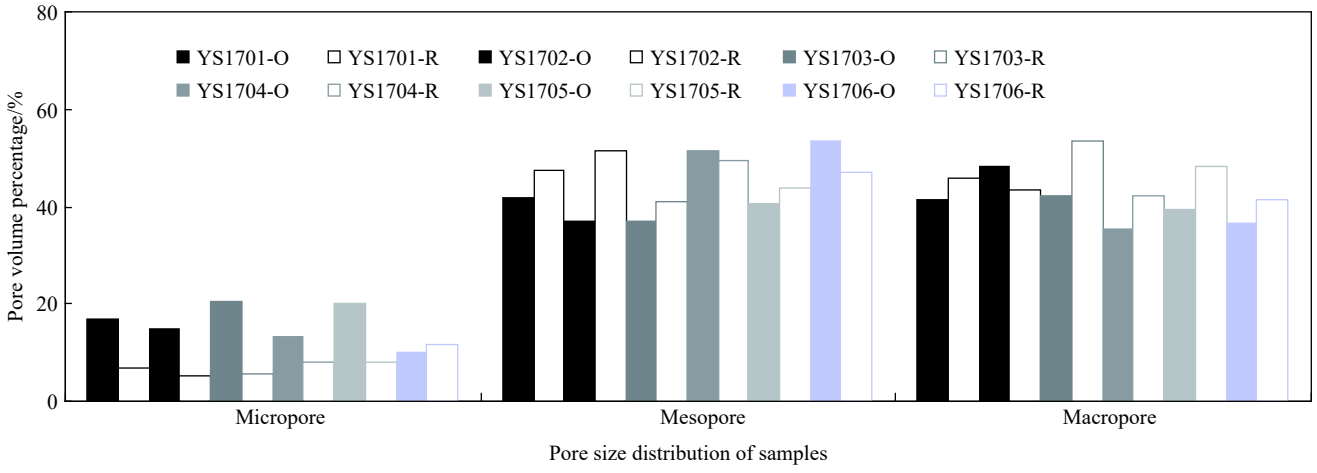

Fig. 6. The average cumulative pore volume of different pore diameter ranges was calculated by the DFT model for original and residual-gas released shale samples. The cumulative pore volume of meso- and macro-pore showed an increasing trend with residual-gas releasing, while the micropore pore volume decreased.

structure. After the crushing process, the shale was excessively crushed and refined to 100–200 mesh, the residual gas released and some of the ink bottle-shaped pores and inclusions type pores are released (Fig. 8a, b). This process is happening to the reservoir evaluation sample processing, where excessive fragmentation and refinement results in the acquisition of a large amount of invalid pore space.

The present study of the effect of residual gas release on pore structure, by the crush method, showed that with the decrease of particle size, the residual gas released by crushing have a different composition to gas produced in the gas field by hydraulic fracturing. The results suggested that the residual gas and its pore space are difficult to be modified and released by hydraulic fracturing. Meanwhile, under the influence of multi-phase basin evolution and tectonic rebuilding processes, such residual gas and pores were widespread in the Longmaxi shale in Southern China (Liang ML et al., 2017; He JL et al., 2018; Gao J et al., 2015, 2017). However, these residual gas do not contribute to shale gas production and these pores are unsuitable for the evaluation of effective pore structure of shale gas reservoirs in the Longmaxi shale. Therefore, the effect of residual gas on pore structure should be considered and the impact of particle size on the pore structure of the Longmaxi shale should be re-examined to avoid the excessive

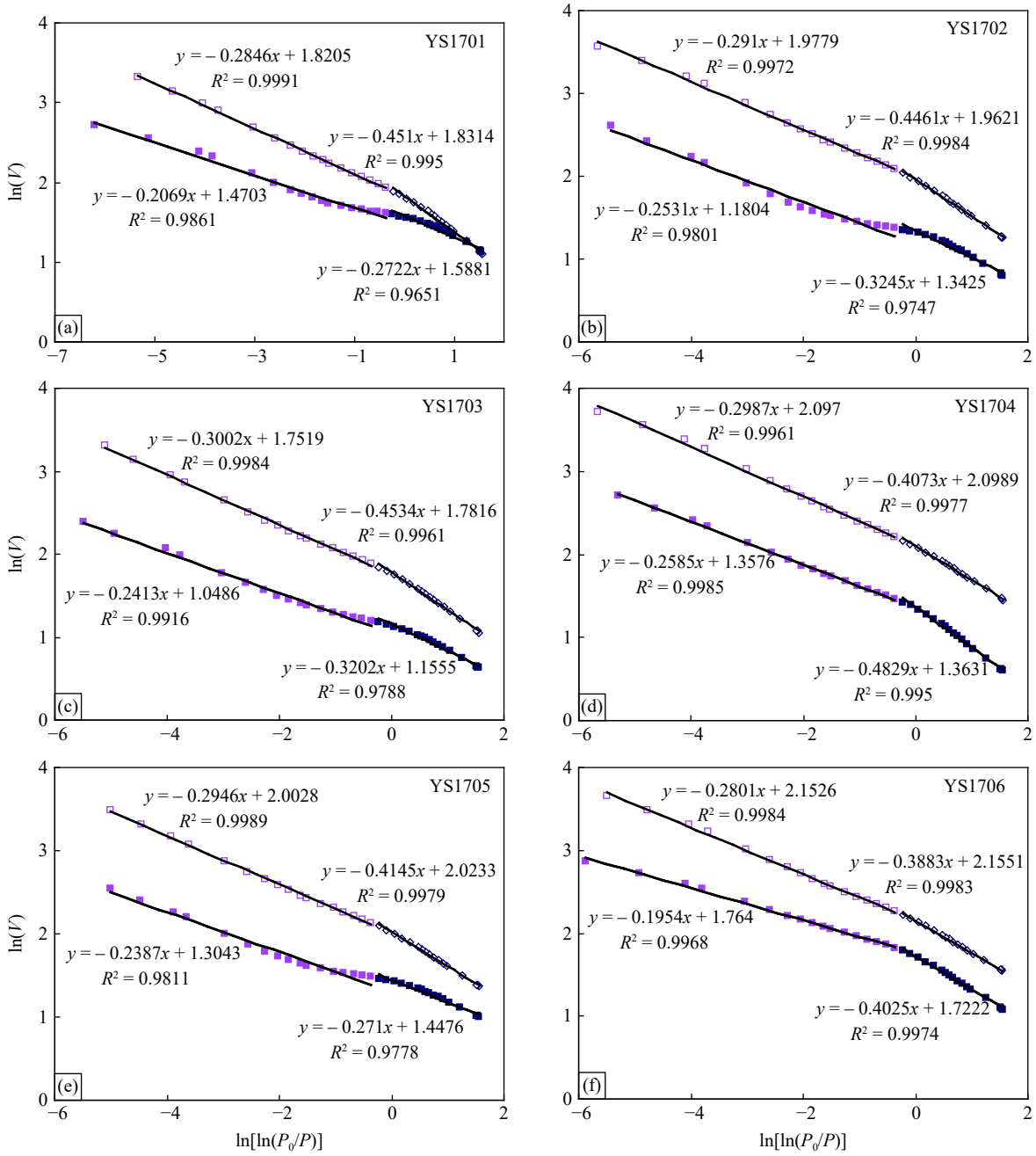

Fig. 7. Plots of ln(*V*) *vs.* ln[ln(P_0/*P*)] were reconstructed from the nitrogen adsorption isotherms for all shale samples in this study. The original shale samples marked as solid-symbol and residual-gas released samples as open-symbol for all samples (a–f). The plots of residual-gas released samples always above the original samples for all shale samples (a–f).

Table 5. Fractal dimensions were derived from the fractal FHH model of shale samples.

Sample	Original shale						Residual gas released shale					
	P/P_0=0–0.5			P/P_0=0.5–1			P/P_0=0–0.5			P/P_0=0.5–1		
	Fitting equation	R^2	D_1	Fitting equation	R^2	D_2	Fitting equation	R^2	D_1	Fitting equation	R^2	D_2
YS1701	y=−0.2722x+1.5881	0.9651	2.7278	y=−0.2069x+1.4703	0.9861	2.7931	y=−0.451x+1.8314	0.9950	2.5490	y=−0.2846x+1.8205	0.9991	2.7154
YS1702	y=−0.3245x+1.3425	0.9747	2.6755	y=−0.2531x+1.1804	0.9801	2.7469	y=−0.4461x+1.9621	0.9984	2.5539	y=−0.291x+1.9779	0.9972	2.7090
YS1703	y=−0.3202x+1.1555	0.9788	2.6798	y=−0.2413x+1.0486	0.9916	2.7587	y=−0.4534x+1.7816	0.9961	2.5466	y=−0.3002x+1.7519	0.9984	2.6998
YS1704	y=−0.4829x+1.3631	0.9950	2.5171	y=−0.2585x+1.3576	0.9985	2.7415	y=−0.4073x+2.0989	0.9977	2.5927	y=−0.2987x+2.097	0.9961	2.7013
YS1705	y=−0.271x+1.4476	0.9778	2.7290	y=−0.2387x+1.3043	0.9811	2.7613	y=−0.4145x+2.0233	0.9979	2.5855	y=−0.2946x+2.0028	0.9989	2.7054
YS1706	y=−0.4025x+1.7222	0.9974	2.5975	y=−0.1954x+1.764	0.9968	2.8046	y=−0.3883x+2.1551	0.9983	2.6117	y=−0.2801x+2.1526	0.9984	2.7199

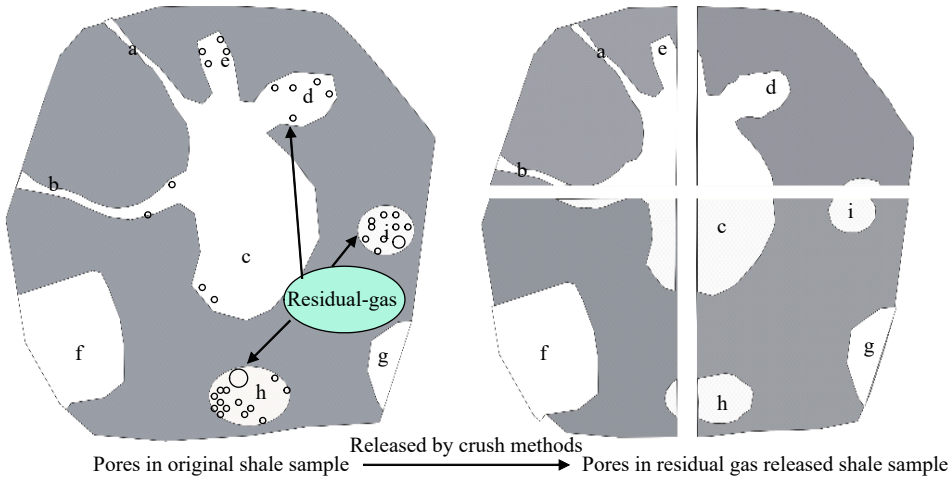

Fig. 8. The schematic diagram shows the change of the original pore structure and the pore connectivity network influenced by residual gas releasing and particle crushing. Pores in the original shale sample were: a, b–micropores; c–macropores; d, e–mesopores; f, g–opened pores of meso- and macropore; h, i–closed pores. Pores in residual gas released shale sample was opened pores, characterized and dominated on meso- and macropore.

pursuit of understanding pore structure at all scales, rather than the effectiveness of pore structure for gas production in future studies. Crushing of shale not only alters the particle size but also released residual-gas and previously closed pores to gas production. Excessive refinement will affect the original effective pore structure of the shale (Li B et al., 2019), and crushing might introduce artificial pores due to the opening of otherwise closed pores (Yu YX et al., 2019). It has been concluded that the 20 –35 mesh of particle size was recommended because of the best agreement between helium porosity and mercury/N_2 porosity for shale samples (Comisky JT et al., 2011). In the present study, the authors give more evidence that large-diameter samples are more reasonable for shale reservoir evaluation. Both the residual gas and their pore space have no contribution to shale gas production and effective reservoir evaluation. The larger fragments samples of granular rather than powdery smaller than 60 mesh fraction of shale seem to be optimal for performing effective pore structure analysis to the Longmaxi shale.

4. Conclusions

Shale samples from the Longmaxi Formation in the Upper Yangtze, Southern China have been studied and the residual gas was collected by a vacuum crush method. The geochemical compositions of residual gas and the pore structure of both the original and post-residual gas released shale samples were analyzed. The following main conclusions have been reached:

(i) A variety of residual gas were released from all six Longmaxi shale samples, though dominated by CH_4 and CO_2, and of different geochemical composition to the produced gas from Longmaxi shale after hydraulic fracturing.

(ii) Release of residual gas affects pore structure. Crushing and gas releasing of shale improved the surface area and adsorption capacity of shale and increased the pores with pore size from 10–80 nm and 100–200 nm.

(iii) Proposed influence mechanisms which can explain the effect of residual gas released on pore structure by crush methods: (1) Residual gas of adsorbent gas released from organic matter-related pores and (2) residual gas of inclusion

gas released from closed pores.

The research expands the scope of material composition affecting pore structure in gas shale and makes it more reasonable that the effect of particle size on pore structure. It is should consider that those residual gas and its related pore spaces obtained by excessive crushing are meaningless for the evaluation and production of shale gas reservoirs. The larger fragments samples of granular rather than powdery smaller than 60 mesh fraction of shale seem to be better for performing effective pore structure analysis to the Longmaxi shale.

CRediT authorship contribution statement

Ming-liang Liang, Zong-xiu Wang conceived of the presented idea. Ming-liang Liang wrote the manuscript with support from Guo-dong Zheng and Hugh Christopher Greenwell. Hui-jun Li, Lin-yan Zhang, Xing-qiang Feng and Kai-xun Zhang helped supervise the project. All authors discussed the results and contributed to the final manuscript.

Declaration of competing interest

The authors declare no conflict of interest.

Acknowledgment

This work was financially supported by the National Natural Science Foundation of China (41802158), projects of China Geological Survey (DD20160183, DD20190085), Major State Research Development Program of China (2016YFC0600202), Fundamental Research Funds for Chinese Academy of Geological Sciences (JYYWF20181201) and the CGS-CSC Scholarship Fund (201908575013).

References

Barrett EP, Joyner LG, Halenda PP. 1951. The determination of pore volume and area distributions in porous substances. I. Computations from nitrogen isotherms. Journal of the American Chemical Society, 73, 373–380. doi: 10.1021/ja01145a126.

Cao TT, Song ZG, Wang SB, Xia J. 2016. Characterization of pore structure and fractal dimension of Paleozoic shales from the northeastern Sichuan Basin, China. Journal of Natural Gas Science and Engineering, 35, 882–895. doi: 10.1016/j.jngse.2016.09.022.

Cao CH, Zhang MJ, Tang QY, Lü ZG, Wang Y, Du L, Li ZP. 2015. Geochemical characteristics and implications of shale gas in Longmaxi formation, Sichuan Basin, China. Natural Gas Geoscience, 26, 1604–1612 (in Chinese with English abstract).

Clarkson CR, Haghshenas B, Ghanizadeh A, Qanbari F, Williams-Kovacs JD, Riazi N, Debuhr C, Deglint HJ. 2016. Nanopores to megafractures: Current challenges and methods for shale gas reservoir and hydraulic fracture characterization. Journal of Natural Gas Science and Engineering, 31, 612–657. doi: 10.1016/j.jngse.2016.01.041.

Chalmers GRL, Bustin RM. 2007. The organic matter distribution and methane capacity of the Lower Cretaceous strata of Northeastern British Columbia, Canada. International Journal of Coal Geology, 70, 223–239. doi: 10.1016/j.coal.2006.05.001.

Chalmers GRL, Bustin RM. 2008. Lower Cretaceous gas shales in Northeastern British Columbia, Part I: Geological controls on methane sorption capacity. Bulletin of Canadian Petroleum Geology, 56, 1–21. doi: 10.2113/gscpgbull.56.1.1.

Chalmers GRL, Ross DJK, Bustin RM. 2012. Geological controls on matrix permeability of Devonian Gas Shales in the Horn River and Liard basins, northeastern British Columbia, Canada. International Journal of Coal Geology, 103, 120–131. doi: 10.1016/j.coal.2012.05.006.

Chen TY, Feng XT, Pan ZJ. 2015. Experimental study of swelling of organic rich shale in methane. International Journal of Coal Geology, 150, 64–73. doi: 10.1016/j.coal.2015.08.001.

Chen F, Lu S, Ding X. 2018. Pore types and quantitative evaluation of pore volumes in the Longmaxi Formation shale of Southeast Chongqing, China. Acta Geologica Sinica (English edition), 92, 342–353. doi: 10.1111/1755-6724.13509.

Comisky JT, Santiago M, McCollom B, Buddhala A, Newsham KE. 2011. Sample size effects on the application of mercury injection capillary pressure for determining the storage capacity of tight gas and oil shales. Society of Petroleum Engineers, SPE-149432-MS. doi: 10.2118/149432-MS.

Curtis JB. 2002. Fractured shale-gas systems. AAPG Bulletin, 86, 1921–1938. doi: 10.1306/61EEDDBE-173E-11D7-8645000102C1865D.

Curtis ME, Cardott BJ, Sondergeld CH, Rai CS. 2012. Development of organic porosity in the Woodford Shale with increasing thermal maturity. International Journal of Coal Geology, 103, 26–31. doi: 10.1016/j.coal.2012.08.004.

Dai JX, Zou CN, Liao SM, Dong DZ, Ni YY, Huang JL, Wu W, Gong DY, Huang SP, Hu GY. 2014. Geochemistry of the extremely high thermal maturity Longmaxi shale gas, southern Sichuan Basin. Organic Geochemistry, 74, 3–12. doi: 10.1016/j.orggeochem.2014.01.018.

Gao J, He S, Yi JZ. 2015. Discovery of high density methane inclusions in Jiaoshiba shale gas field and its signigicance. Oil and Gas Geology, 36, 472–482 (in Chinese with English abstract).

Gao J, He S, Zhao JX, Yi JZ. 2017. Geothermometry and geobarometry of overpressured lower Paleozoic gas shales in the Jiaoshiba field, Central China: Insight from fluid inclusions in fracture cements. Marine and Petroleum Geology, 83, 124–139. doi: 10.1016/j.marpetgeo.2017.02.018.

Gao L, Wang ZX, Liang ML, Yu YX, Zhou L. 2018. Experimental study of the relationship between particle size and methane sorption capacity in shale. Journal of Visualized Experiments, e57705. doi: 10.3791/57705.

Guo TL. 2016. Discovery and characteristics of the Fuling shale gas field and its enlightenment and thinking. Earth Science Frontiers, 23, 29–43 (in Chinese with English abstract).

Groen JC, Peffer LAA, Perez-Ramírez J. 2003. Pore size determination in modified micro- and mesoporous materials. Pitfalls and limitations in gas adsorption data analysis. Microporous and Mesoporous Materials, 60, 1–17. doi: 10.1016/S1387-1811(03)00339-1.

He JL, Wang J, Yu Q, Liu W, Ge XY, Yang P, Zang ZJ, Lu JZ. 2018. Pore structure of shale and its effects on gas storage and transmission capacity in well HD-1 eastern Sichuan Basin, China. Fuel, 226, 709–720. doi: 10.1016/j.fuel.2018.04.072.

Horvath G, Kawazoe K. 1983. Method for the calculation of effective pore-size distribution in molecular-sieve carbon. Journal of Chemical Engineering of Japan, 16, 470–475. doi: 10.1252/jcej.16.470.

Ismail IMK, Pfeifer P. 1994. Fractal analysis and surface roughness of nonporous carbon fibers and carbon blacks. Langmuir, 10, 1532–1538. doi: 10.1021/la00017a035.

Jaroniec M. 1995. Evaluation of the fractal dimension from a single adsorption isotherm. Langmuir, 11, 2316–2317. doi: 10.1021/la00006a076.

Ju YW, Sun Y, Tan JQ, Bu HL, Han K, Li XS, Fang LZ. 2018. The composition, pore structure characterization and deformation mechanism of coal-bearing shales from tectonically altered coalfields in eastern China. Fuel, 234, 626–642. doi: 10.1016/j.fuel.2018.06.116.

Li B, Chen FW, Xiao DS, Lu SF, Zhang LC, Zhang YY, Gong C. 2019. Effect of partical size on the experiment of low temperature nirogen adsorption: A case study of marine gas shale in Wufeng-Longmaxi formation. Journal of China University of Mining & Technology, 48(2), 367–376 (in Chinese with English abstract).

Li LW, Liu Y, Wang XB, Zhang MJ, Cao CH, Xing LT, Li ZP. 2017. Development of a combined device with high vacuum and pulsed discharge gas chromatography and its application in chemical analysis of gas from rock samples. Rock and Mineral Analysis, 36, 222–230 (in Chinese with English abstract).

Li LW, Cao CH, He J, Xing LT, Li ZP, Du L. 2015. Combined analysis system and its apply method of high vacuum rock degassing and gas chromatography. CN201410746067.X.

Li J, Zhou SX, Li YJ, Ma Y, Yang YN, Li CC. 2016. Effect of organic matter on pore structure of mature lacustrine organic-rich shale: A case study of the Triassic Yanchang shale, Ordos Basin, China. Fuel, 185, 421–431. doi: 10.1016/j.fuel.2016.07.100.

Liang ML, Wang ZX, Gao L, Li CL, Li HJ. 2017. Evolution of pore structure in gas shale related to structural deformation. Fuel, 197, 310–319. doi: 10.1016/j.fuel.2017.02.035.

Luo L, Ya OW, Liu JX, Zhang H, Ma JF, Jiang XM. 2019. The effect of the grinding process on pore structures, functional groups and release characteristic of flash pyrolysis of superfine pulverized coal. Fuel, 235, 1337–1346. doi: 10.1016/j.fuel.2018.08.081.

Luo QY, Zhong NN, Dai N, Zhang W. 2016. Graptolite-derived organic matter in the Wufeng-Longmaxi Formations (Upper Ordovician – Lower Silurian) of southeastern Chongqing, China: Implications for gas shale evaluation. International Journal of Coal Geology, 153, 87–98. doi: 10.1016/j.coal.2015.11.014.

Loucks RG, Reed RM, Ruppel SC, Jarvie DM. 2009. Morphology, genesis, and distribution of nanometer-scale pores in siliceous mudstones of the Mississippian Barnett Shale. Journal of Sedimentary Research, 79, 848–861. doi: 10.2110/jsr.2009.092.

Loucks RG, Reed RM, Ruppel SC, Hammes U. 2012. Spectrum of pore types and networks in mudrocks and a descriptive classification for matrix-related mudrock pores. AAPG Bulletin, 96, 1071–1098. doi: 10.1306/08171111061.

Mastalerz M, Hampton L, Drobniak A, Loope H. 2017. Significance of analytical particle size in low-pressure N_2 and CO_2 adsorption of coal and shale. International Journal of Coal Geology, 178, 122–131. doi: 10.1016/j.coal.2017.05.003.

Mahamud MM, Novo MF. 2008. The use of fractal analysis in the textural characterization of coals. Fuel, 87, 222–231. doi: 10.1016/j.fuel.2007.04.020.

Meng FY, Li SZ, Wei SY, Zhang SS, Wang P, Wang C. 2020. Discovery of shale gas from Wufeng-Longmaxi Formation in Xianfeng area, Hubei Province, China. China Geology, 3, 493–495. doi: 10.31035/cg2020030.

Milkov AV, Faiz M, Etiope G. 2020. Geochemistry of shale gas from around the world: Composition, origins, isotope reversals and rollovers, and implications for the exploration of shale plays. Organic Geochemistry, 143, 103997. doi: 10.1016/j.orggeochem.2020.103997.

Nie HK, Tang X, Bian RK. 2009. Congtrolling factors for shale gas accumulation and prediction of potential development area in shale gas reservoir of South China. Acta Petrolei Sinica, 30, 484–491 (in Chinese with English abstract).

Qi H, Ma J, Wong P. 2002. Adsorption isotherms of fractal surfaces. Colloids and Surfaces A: Physicochemical and Engineering Aspects, 206, 401–407. doi: 10.1016/S0927-7757(02)00063-8.

Rouquerol F, Rouquerol J, Sing K. 1999. Adsorption by Powders and Porous Solids. US, Academic Press, 1–467.

Ross DJK, Bustin RM. 2007. Shale gas potential of the Lower Jurassic Gordondale member, Northeastern British Columbia, Canada. Bulletin of Canadian Petroleum Geology, 55, 51–75. doi: 10.2113/gscpgbull.55.1.51.

Ross DJK, Bustin RM. 2008. Characterizing the shale gas resource potential of Devonian –Mississippian strata in the Western Canada sedimentary basin: Application of an integrated formation evaluation. AAPG Bulletin, 92, 87–125. doi: 10.1306/09040707048.

Ross DJK, Bustin RM. 2009. The importance of shale composition and pore structure upon gas storage potential of shale gas reservoirs. Marine and Petroleum Geology, 26, 916–927. doi: 10.1016/j.marpetgeo.2008.06.004.

Sun LN, Tuo JC, Zhang MF, Wu CJ, Wang ZX, Zheng YW. 2015. Formation and development of the pore structure in Chang 7 member oil-shale from Ordos Basin during organic matter evolution induced by hydrous pyrolysis. Fuel, 158, 549–557. doi: 10.1016/j.fuel.2015.05.061.

Sing KSW, Everett DH, Haul RAW. 1985. Reporting physisorption data for gas/solid systems with special reference to the determination of surface area and porosity. Pure and Applied Chemistry, 57, 603–619. doi: 10.1351/pac198557040603.

Tan JQ, Weniger P, Krooss B, Merkel A, Horsfield, Zhang JC, Boreham CJ, Graas G, Tocher BA. 2014. Shale gas potential of the major marine shale formations in the Upper Yangtze Platform, South China, Part II: Methane Sorption Capacity. Fuel, 129, 204–218. doi: 10.1016/j.fuel.2014.03.064.

Thommes M, Kaneko K, Neimark AV, Olivier JP, Rodriguez-Reinosooo F, Rouquerol J, Sing KSW. 2015. Physisorption of gas, with special reference to the evaluation of surface area and pore size distribution (IUPAC Technical Report). Pure and Applied Chemistry, 87, 1051–1069. doi: 10.1515/pac-2014-1117.

Wan JB, He XF, Liu M. 2015. Shale gas content measurement and calculation method. Well logging Technology, 39, 756–761 (in Chinese with English abstract).

Wang QT, Shen CC, Chen Q, Zhang L, Lu H. 2015. Pore characteristics and gas released by crush methods of Wufeng-Longmaxi shale in the northwest of Hubei Province, China. Acta Geologica Sinica (English edition), 89, 93–96. doi: 10.1111/1755-6724.12302_40.

Wu CJ, Tuo JC, Zhang MF, Sun LN, Qian Y, Liu Y. 2016. Sedimentary and residual gas geochemical characteristics of the Lower Cambrian organic-rich shales in Southeastern Chongqing, China. Marine and Petroleum Geology, 75, 140–150. doi: 10.1016/j.marpetgeo.2016.04.013,.

Yang YR, Liu XC, Zhang H, Zhai GY, Zhang JD, Hu ZF, Bao SJ, Zhang C, Wang XH, Yang X, Liu ZZ, Xie T, Chen J, Fang LY, Qin LJ. 2019. A review and research on comprehensive characterization of microscopic shale gas reservoir space. China Geology, 2, 541–556. doi: 10.31035/cg2018116.

Yao YB, Liu DM, Tang DZ, Tang SH, Huang WH. 2008. Fractal characterization of adsorption-pores of coals from North China: An investigation on CH_4 adsorption capacity of coals. International Journal of Coal Geology, 73, 27–42. doi: 10.1016/j.coal.2007.07.003.

You SG, Guo Q, Geng XJ. 2015. Factors affecting the shale gas content and gas content testing methods. China Mining Magazine, 24, 80–85 (in Chinese with English abstract).

Yu YX, Luo XR, Wang ZX, Cheng M, Lei YH, Zhang LK, Yin JT. 2019. A new correction method for mercury injection capillary pressure (MICP) to characterize the pore structure of shale. Journal of Natural Gas Science and Engineering, 68, 102896. doi: 10.1016/j.jngse.2019.05.009.

Zhai GY, Wang YF, Zhou Z, Yu SF, Chen XL, Zhang YX. 2018a. Exploration and research progress of shale gas in China. China Geology, 1, 257–272. doi: 10.31035/cg2018024.

Zhai GY, Wang YF, Zhou Z, Liu GH, Yang YR, Li J. 2018b. “Source-Diagenesis-Accumulation” enrichment and accumulation regularity of marine shale gas in southern China. China Geology, 1, 319–330. doi: 10.31035/cg2018059.

Zhang TW, Ellis G, Ruppel S, Milliken K, Yang RS. 2012. Effect of organic-matter type and thermal maturity on methane adsorption in shale-gas systems. Organic Geochemsitry, 47, 120–131. doi: 10.1016/j.orggeochem.2012.03.012.

Zhang TW, Yang RS, Milliken KL, Ruppel SC, Pottorf RJ, Sun X. 2014. Chemical and isotopic composition of gas released by crush methods from organic rich mudrocks. Organic Geochemsitry, 73, 16–28. doi: 10.1016/j.orggeochem.2014.05.003.

Zhou Z, Bao SJ, Chen XL, Yu SF, Chen K, Guo TX, Xu QF. 2018. A discovery of Silurian tight shale gas in Jianshi, Hubei, China. China Geology, 1, 160–161. doi: 10.31035/cg2018014.